Flight Tests of a Remaining Flying Time Prediction System for Small Electric Aircraft in the Presence of Faults

Edward F. Hogge[1], Chetan S. Kulkarni[2], Sixto L. Vazquez[3], Kyle M. Smalling[4], Thomas H. Strom[5], Boyd L. Hill[6], and Cuong C. Quach[7]

[1,4,5]*Northrop Grumman Technology Services, NASA Langley Research Center, Hampton, Virginia 23681*
edward.f.hogge@nasa.gov
kyle.m.smalling@nasa.gov
thomas.h.strom@nasa.gov

[2]*Stinger Ghaffarian Technologies, Inc., NASA Ames Research Center, Moffett Field, California 94035*
chetan.s.kulkarni@nasa.gov

[3,7]*NASA Langley Research Center, Hampton, Virginia 23681*
sixto.l.vazquez@nasa.gov
cuong.c.quach@nasa.gov

[6]*Analytical Mechanics Associates, Inc., NASA Langley Research Center, Hampton, Virginia 23681*
boyd.l.hill@nasa.gov

ABSTRACT

This paper addresses the problem of building trust in the online prediction of a battery powered aircraft's remaining flying time. A series of flight tests is described that make use of a small electric powered unmanned aerial vehicle (eUAV) to verify the performance of the remaining flying time prediction algorithm. The estimate of remaining flying time is used to activate an alarm when the predicted remaining time is two minutes. This notifies the pilot to transition to the landing phase of the flight. A second alarm is activated when the battery charge falls below a specified limit threshold. This threshold is the point at which the battery energy reserve would no longer safely support two repeated aborted landing attempts. During the test series, the motor system is operated with the same predefined timed airspeed profile for each test. To test the robustness of the prediction, half of the tests were performed with, and half were performed without, a simulated powertrain fault. The pilot remotely engages a resistor bank at a specified time during the test flight to simulate a partial powertrain fault. The flying time prediction system is agnostic of the pilot's activation of the fault and must adapt to the vehicle's state. The time at which the limit threshold on battery charge is reached is then used to measure the accuracy of the remaining flying time predictions. Accuracy requirements for the alarms are considered and the results discussed.

1. INTRODUCTION

Improvements in battery storage capacity have made it possible for general aviation vehicle manufacturers to consider electrically-powered solutions. The development of trust in battery remaining operating time estimates, however, is currently a significant obstacle when considering adoption of electrical propulsion systems in aircraft (Patterson, German & Moore, 2012). There are several ways in which predicting remaining operating time is more complicated for battery-powered vehicles than it is for vehicles with a conventionally-powered liquid-fueled combustion system. Unlike a liquid-fueled system, where the fuel tank's volume remains unchanged over successive refueling procedures, a battery's charge storage capacity will diminish over time. Another complicating feature of a battery system is the time-varying relationship between battery output power and battery current draw. Whereas a conventional liquid combustion system uses an approximately constant amount of liquid fuel to produce a given motive power, the power from a battery system is equal to the product of battery voltage and current. Thus, as batteries are discharged, their voltages drop, and they will lose charge at a faster rate.

Previous papers introduced several new tools for battery discharge prediction onboard a small electric aircraft. A series of ground tests similar to the flight tests used in this

work are described in Hogge, Bole, Vazquez, Celaya, Strom, Hill, Smalling & Quach (2015), and a battery equivalent circuit model used to simulate the battery state is described in Bole, Teubert, Quach, Hogge, Vazquez and Goebel (2013). The model's battery capacity, internal resistance and other parameters were identified through two laboratory experiments that used a programmed load. In one experiment the batteries were slowly discharged. In the other experiment a repeated pulsed loading discharge was done. Current and voltage profiles logged during flights of a small electric airplane further tuned the battery model (Quach, Bole, Hogge, Vazquez, Daigle, Celaya, Weber & Goebel, 2013). The use of a flight plan with upper and lower uncertainty bounds on the required energy to complete the mission successfully was presented along with an approach to identify additional parasitic battery loads (Bole, Daigle & Gorospe, 2014). This paper describes results of initial flight tests to assess the performance of an alarm that warns system operators when the estimated remaining flying time falls below a certain threshold.

A large electric unmanned aerial vehicle (eUAV) was used in this study. The eUAV is a 33% sub-scale version of the Zivko Aeronautics Inc. Edge 540T tandem seat aerobatic aircraft as seen in Fig. 1. This vehicle has been actively used by researchers at NASA Langley Research Center to facilitate the rapid deployment and evaluation of Battery Health Management algorithms for electric aircraft since 2010. Examples of prior works using this platform are found in the following papers: (Saha, Koshimoto, Quach, Hogge, Strom, Hill, Vazquez & Goebel, 2011), (Hogge, Quach, Vazquez & Hill, 2011) and (Daigle, Saxena & Goebel, 2012).

Remaining flying time prediction algorithms focus on the prediction of battery charge depletion over an eUAV flight. A lower-bound on the battery state of charge (SOC) that is considered safe for flight is set at 30% in this work. Flying the vehicle with batteries below 30% SOC is considered to be a high-risk mode of operation. Policy and guidelines are set according to the rulings and the engineering judgment of the NASA Langley UAS Operations Office and the NASA Langley Airworthiness and Safety Review Board. Such violations of operating guidelines are referred to here as a functional failure of the vehicle's mission. The primary use case for remaining flying time predictions is to warn system operators when landing procedures must be initiated to avoid the aircraft motor batteries becoming too depleted. Ground based tests of a typical "missed approach" maneuver were made in a laboratory test facility. It was determined that initiating landing procedures when the eUAV batteries reach 30% SOC would provide a sufficient energy buffer for at least two "missed approach" maneuvers without risk of exceeding battery current limits and the risk of excessive heating based upon ground tests. The predictive element to be tested in this work is an alarm that warns system operators when the powertrain batteries are within two minutes of reaching the 30% SOC threshold under normal operating conditions. This should allow the pilot sufficient time to prepare for landing without exceeding a moderate work load.

Figure 1. The Edge 540T Rapid Evaluation eUAV

The accuracy of onboard remaining flying time estimation algorithms was tested in this work. A series of controlled run-to-functional-failure (charge depletion) flight experiments were conducted while a ground station operator monitored the battery health parameters. The vehicle under test was flown by a pilot experienced in flying large radio control models. The pilot followed a flight plan of timed constant airspeed cruise legs.

The time it took for powertrain batteries to reach 30% SOC established a truth value for the functional failure time. Ground based tests established confidence in the battery SOC diagnostic where the powertrain batteries could be repeatedly run down to their lower-limits without risking loss of the vehicle (Hogge et al., 2015).

The defined performance requirements were then verified by repeating ground based run-to-functional-failure tests a specified number of times previously reported in Hogge et al. (2015). The performance requirement testing procedure used here was originally introduced in Saxena, Roychoudhury, Lin and Goebel (2013).

Section 2 of this paper provides an overview of the Edge 540T powertrain. Algorithms used for onboard battery state estimation and remaining flying time predictions are summarized in Section 3. The process used to verify onboard remaining flying time predictions through structured flight tests and experimental results are described in Section 4. Finally, concluding remarks are given in Section 5.

2. OVERVIEW OF EDGE 540T POWERTRAIN

A wiring diagram for the vehicle powertrain is shown in Fig. 2. The aircraft has two 3-phase tandem motors that are mechanically coupled to the aircraft propeller. Powertrain batteries are arranged in two pairs of series connected battery

packs. A switchable parasitic load R_p injects a fault to test the robustness of the remaining flying time estimation algorithms to changes in the battery loading demand. The other symbols in the figure identify the location of the current and voltage sensors.

Remaining flying time predictions are generated by propagating a number of estimates of the battery charge forward. Forward propagation of the present battery state estimate is performed using an estimate of the future powertrain demand that will occur over the known flight plan. These future loads include propeller loads and parasitic loads. The prognostic tools make use of the known flight plan to inform future load predictions, but no prior information is assumed to be available regarding when a parasitic load may be injected.

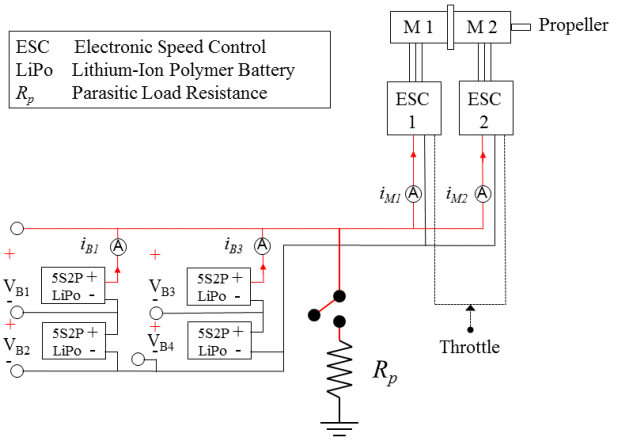

Figure 2. Schematic of electric Powertrain.

3. REMAINING FLYING TIME PREDICTION

Battery discharge prediction is described here in terms of the following components; (i) online battery state estimation; (ii) prediction of future battery power demand as a function of an aircraft flight plan; (iii) online estimation of additional parasitic battery loads; and (iv) prediction of battery discharge over the future flight plan. The assumptions and algorithms used for each of these steps are summarized in this section.

3.1. Online Battery State Estimation

Our previous papers (Quach et al., 2013) and (Bole et al., 2014), described the use of an equivalent circuit model and unscented Kalman filtering (UKF) (Julier & Uhlmann, 1997, 2004) to update battery state estimates based on observations of current and voltage at the battery output terminals. This approach is also summarized here for convenience. The state space model of the battery has internal states that are affected by the current withdrawn and the voltage produced at the output terminals (the charge states of each of the capacitors in the equivalent circuit model). The battery state is modeled

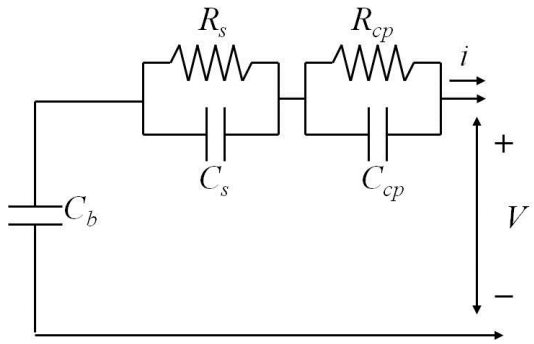

Figure 3. Lithium-Ion battery equivalent circuit model

in a filtering framework that can be used to propagate the battery state in a structured way so as to account for variation in its available current and voltage based upon internal chemical reactions and past usage demand. A Kalman filter is a mathematical framework that captures many aspects of the state tracking problem in an optimal way. It provides a way to represent the uncertainty associated with the state of the battery and measurements in the presence of sensor noise. The unscented Kalman filter uses a mechanism, the unscented transform (UT) to approximate how the state's mean and covariance transform through the nonlinear battery model by maintaining the mean and second moment of the state probability distributions before the nonlinearity and after the nonlinearity. The UT takes a random variable $\mathbf{x}$ with mean $\bar{\mathbf{x}}$ and covariance $\mathbf{P}_{xx}$ that is related to a second random variable $\mathbf{y}$ by some function $\mathbf{y} = \mathbf{g}(\mathbf{x})$ with mean $\bar{\mathbf{y}}$ and covariance $\mathbf{P}_{yy}$ computed with high accuracy using a minimal set of weighted samples called *sigma points* (Julier & Uhlmann, 1997). This special set of points serves as a proxy for the actual battery state probability distribution transformed by the nonlinear battery model and does so more efficiently than other methods. The propagated *sigma points* are used by the UKF to estimate the next battery state from the state population mean and covariance. See Bole et al, 2014 and Daigle et al, 2012 for further information.

Figure 3 shows an equivalent circuit battery model that is used to represent battery output voltage dynamics as a function of the battery current control input. The basic model is based on Thevenin's theorem to model the current and voltage profile of the battery as a black box input-output device. We make the first-approximation assumption that the battery state can match a linear electrical network with voltage and current sources and only resistances. It is similar to models presented in Chen and Rincon-Mora (2006), and Ceralo (2000). This battery model contains six electrical components that are tuned to recreate the observed current-voltage dynamics of the Edge 540T battery packs. The bulk of the battery charge is assumed to be stored in the capacitor C_b. The (R_s, C_s) and (R_{cp}, C_{cp}) circuit element pairs are used to simulate standard battery phenomenon, such as internal resistance drops and hysteresis effects (Saha, Quach &

Goebel, 2012). The ratio of a battery's charge at a given instant to its maximum charge storage capacity is typically referred to as the state of charge (SOC). Battery SOC is defined here as:

$$SOC = 1 - \frac{q_{\max} - q_b}{C_{\max}} \quad (1)$$

where q_b represents the charge stored in capacitor C_b, q_{max} is the maximum charge that the battery can hold, and $C_{\max}$ is the maximum charge that can be drawn from the battery in practice. Here, $C_{\max}$ will always be less than q_{max}, due to electrochemical side-reactions that make some portion of a battery's charge carriers unavailable. As the battery ages more of its internal charge will become unavailable because of these side reactions. The $C_{\max}$ parameter must be refitted periodically to capture the aging effect to maintain prediction accuracy. In our experience each battery must be re-characterized after ten recharge cycles with a slow current discharge lab experiment to capture changes in the $C_{\max}$ and the R_s parameters for each motor battery.

Battery input-output dynamics are known to change as a function of internal battery charge. Some of the parameters in the equivalent circuit model are parameterized as functions of battery state of charge (SOC) (Zhang & Chow, 2010). The following SOC parameterizations were used for the C_b, C_{cp}, and R_{cp} parameters in Fig. 3.

$$C_b = C_{Cb0} + C_{Cb1} \cdot SOC + C_{Cb2} \cdot SOC^2 + C_{Cb3} \cdot SOC^3 \quad (2)$$

$$C_{cp} = C_{cp0} + C_{cp1} \cdot \exp(C_{cp2}(SOC)) \quad (3)$$

$$R_{cp} = R_{cp0} + R_{cp1} \cdot \exp(R_{cp2}(SOC)) \quad (4)$$

the coefficients in the parameterized models for C_b, C_{cp}, and R_{cp} must be tuned based on observed current and voltage battery data over a range of battery SOC values.

Two laboratory experiments were used to fit all of the parameters in the equivalent circuit model to the lithium polymer packs used on the Edge-540T. In one test a battery is discharged using a series of current pulses. This experiment exposes voltage dynamics that must be fit by the R_s, C_s and R_{cp}, C_{cp} parameters in the equivalent circuit model. A multidimensional search method such as the downhill simplex method of Nelder-Mead is used to fit a model to the recorded data (Nelder & Mead, 1965). These identified parameters are associated with a selected battery from a batch of batteries of a given chemical formulation. These parameters are assumed to be unvaried across all similar battery packs of a given batch. Any differences in individual batteries due to manufacturing variation is accounted for by adaptation of the battery charge capacity term $C_{\max}$ of the C_b capacitor in the equivalent circuit model. In a second test, $C_{\max}$ is identified by running a slow discharge lab experiment for each battery pack as shown in Fig. 4. During this low current discharge test, the voltage across the C_b capacitor plays a dominate role. Thus, this experiment allows the $C_{\max}$ parameter in the equivalent circuit model to be fitted in isolation, also through use of the Nelder-Mead simplex method (Bole et al., 2014). The equivalent circuit battery model and the UKF state estimation are assumed to do an adequate job of tracking the total charge within the battery over a flight usage profile.

3.2. Prediction of Motor Power Demand as a Function of Aircraft Flight Plan

After estimating battery state, the next step towards predicting remaining flying time is the estimation of motor power demand over the remainder of a given flight plan. The aircraft's flight plan is assumed here to be specified in advance in terms of a fixed set of segments. Each segment includes a desired vehicle airspeed along with an expected duration or other ending condition. An example flight plan is defined here as:

1. **Takeoff and climb to 200 m:**
   Set airspeed to 25 m/s, hold for 1.2 min
2. **Maintain altitude, maintain airspeed:**
   Set airspeed to 23 m/s, hold for 3.0 min
3. **Maintain altitude, increase airspeed:**
   Set airspeed to 25 m/s, hold for 2.0 min
4. **Maintain altitude, decrease airspeed:**
   Set airspeed to 20 m/s, hold for 2.0 min
5. **Maintain altitude, increase airspeed:**
   Set airspeed to 23 m/s, hold until landing is called by monitors on the ground.
6. **Remote control landing: airspeed and** duration may vary widely depending on pilot and environmental conditions.

The energy required for an aircraft to fly the remainder of a given flight plan will necessarily be uncertain due to variation in pilot behavior and environmental conditions. A minimum, maximum, and median motor power demand for each

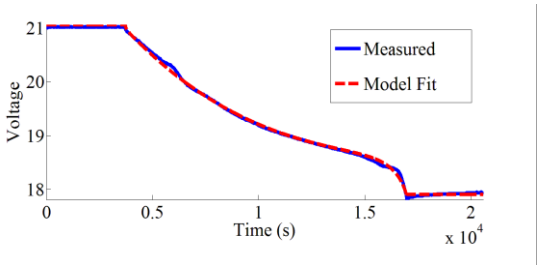

Figure 4. Low-current discharge (2A) lab experiment.

remaining segment of the flight plan is used in this work to represent prediction uncertainty. These three power estimates can then be integrated to form predictions of the minimum, maximum, and median motor energy consumption over the remaining flight plan.

Figure 5 shows sample predictions of future motor power and energy demand over segments 1-5 of the given flight plan. Here, segment 5 of the flight plan is shown to extend out indefinitely (20 minutes), representing the intent to continue flying until the ground team calls for a landing. The median motor power demands are estimated for each flight plan segment using a previously developed model, discussed in Bole et al. (2013) and in Bole et al. (2014). A plus or minus 20% empirically derived error margin around the median motor power demand estimate was used to generate the minimum and maximum predictions shown in Fig. 5 (Saha et al., 2012).

A constraint on the minimum battery SOC required for safely landing the aircraft is considered to limit the aircraft's maximum safe flying time. For safety reasons and for manufacturer's recommendation to optimize battery life, a battery should not be depleted to a very low SOC threshold value. This minimum SOC threshold is considered here to be 30%. Ground static testing of the integrated powertrain and airframe verified that sufficient energy is present to perform two complete "missed approach" landing maneuvers when the SOC is 30%. The ground static tests used the battery voltage and current profiles recorded during typical takeoffs, circling cruise and landing maneuvers. Prediction of available flying time remaining can thus be considered in this example as the time until the battery SOC reaches 30%, assuming that a landing will not be called until the last possible moment. A triplet of minimum, maximum, and median remaining flying time estimates will ultimately be produced by estimating when the battery SOC threshold would be reached for each of the minimum, maximum, and median motor power profiles.

3.3. Online Estimation of Additional Parasitic Battery Loads from an Injected Powertrain Fault

Parasitic demands on the battery system that cannot be known in advance are simulated with a resistive load that may be injected in parallel with the aircraft batteries at any time during flight. Let R_p be the unknown parasitic load. The parasitic current, i_p ,is the difference in the current i measured at the battery and the current i_m measured at the motor controller. The locations of the battery current sensors i_{B1} and i_{B2} for battery current i and the motor current sensors i_{M1} and i_{M2} for motor current i_m are found in Fig. 2. A residual, defined as the difference between an observed signal and its model-predicted value, can be defined for the parasitic fault detection based on the measured values of i and i_m. In the nominal case, our model for i is $i = i_m$. We can then define a residual, r_i, as $r_i = i^* - i_m^*$, where the $*$superscript indicates a measured value. Nominally, $r_i = 0$,and we can define a simple threshold-based fault detector that triggers when $r_i > 0$ for some threshold T. Once a fault is detected, we can estimate the parasitic current at time k using

$$\widehat{i_p}(k) = i^*(k) - i_m^*(k). \quad (5)$$

The parasitic resistance can then be estimated with Ohm's Law

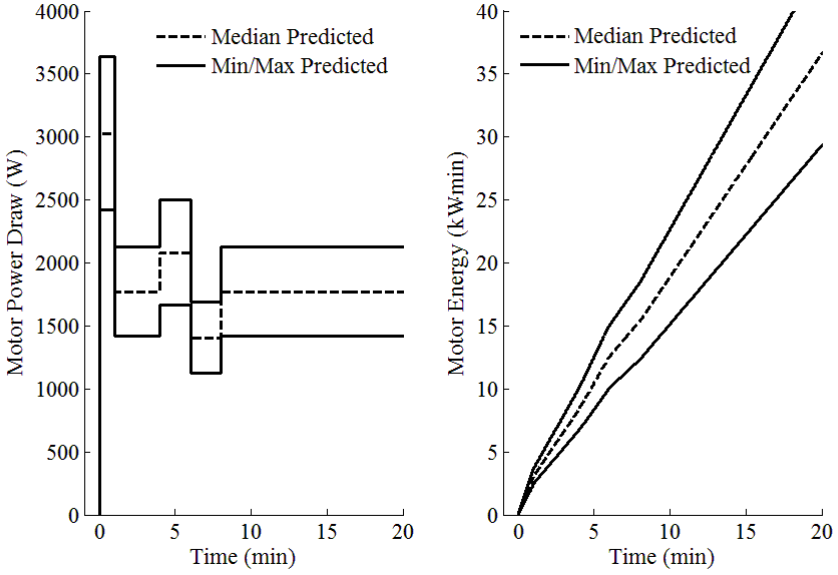

Figure 5. Uncertain predictions of motor power and energy draw over the sample flight plan

$$\widehat{R_p}(k) = \frac{V_b^*(k)}{\widehat{i_p}}. \quad (6)$$

The estimate $\widehat{R_p}$(k) will be noisy, since it is computed based on measured values. Assuming that R_p is constant, we take the median of all computed values to provide a robust estimate of R_p, i.e.,

$$R_p(k) = \text{median}(\{\widehat{R_p}(k_j) : k_d \geq k_j \geq k\}), \quad (7)$$

where k_d is the time of fault detection (and the time that fault identification begins). This online filtering routine is described further in Bole et al. (2014). A battery current profile and parasitic load estimates from a sample aircraft data set is shown in Fig. 6. Here, a 5. 5 Ω parasitic load is injected in parallel with the aircraft batteries at 5 minutes into the flight for half of the test series. At the time the load is injected, the battery current becomes notably higher than the motor current. The estimated parasitic load then rapidly converges to approximately 5.5 Ω. Online parasitic load estimates are directly incorporated into the battery discharge predictions. This results in an immediate shift in the battery discharge predictions each time the parasitic load estimate is updated.

3.4. Prediction of Battery Discharge Over a Flight Plan

The Prognostic Horizon metric defined by Saxena, Celaya, Saha, Saha and Goebel (2010) is the difference in the time when the prediction meets error criteria and the time when the event predicted occurs. It is represented by the symbol λ. The accuracy of that prediction falling within a specified error margin is denoted by the parameter α. The α margin limits are set according to the risk of early prediction and according to the risk of late prediction of the remaining flying time. In our case, the risk posed by late prediction of the time of zero remaining flying time is risk to the vehicle successfully landing. The risk posed by an excessively early prediction is the opportunity cost posed by landing too early and any additional missions needed to accomplish what was missed by landing early. "*The desired level of accuracy with respect to the (remaining flying time) ground truth is specified as ±α bounds*". The tuning of the estimation algorithm biases the prediction of remaining flying time to regard overestimation as a hazardous mode of operation to be avoided (Saxena et al., 2013). Ground Truth from a set of test flights was used to determine the actual remaining flying time on average, and the α^+ margin set to be the same (0%). Since the typical prediction accuracy fell between ±20% error, the early prediction bound α^- was set to 40% to bias the acceptable predictions to be early rather than late. This is reflected in the α^+ limit bound having a value of 0% indicating no tolerance for overestimation of remaining flying time. The α^- limit bound for underestimation of remaining flying time is set to 40% below the ground truth value.

Figure 7 shows predictions of remaining flying time for the example run. The dark line in Fig. 7 denoted in the legend as α^+ indicates the true flying time remaining. The dashed line in Fig. 7 represents the median prediction of flying time remaining. The vertical extent of the histograms represents the interval between the minimum, median and maximum remaining flying time predictions. Here, the predicted remaining flying time is found by subtracting the present time from the time at which the lowest battery SOC crosses the 30% threshold when simulated into the future using the energy demand implied by the projected flight plan. The predictions slightly underestimate remaining flying time until the parasitic load is detected at about 5 minutes into the flight. After the parasitic load is detected the remaining flying time predictions are immediately shifted down and increase the degree of underestimation.

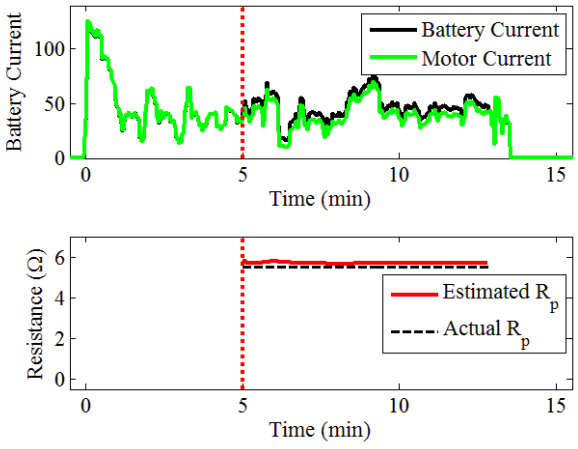

Figure 6. Sample motor and battery current profiles (top), along with parasitic load estimates (bottom)

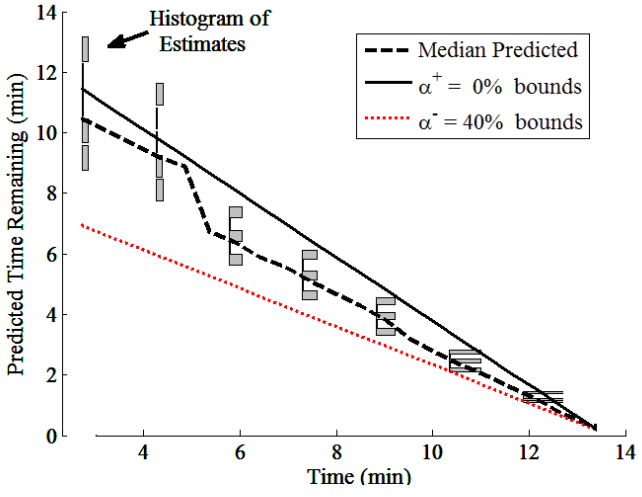

Figure 7. Histograms of predictions of flying time remaining within α limit boundaries

4. FLIGHT TEST VERIFICATION OF REMAINING FLYING TIME PREDICTION

A description of the flight test experiment, followed by the performance requirements, the β metric, the SOC ground truth, SOC and remaining flying time results are found in this section.

The flight test verification of the Edge 540T hardware and software was initiated by loading the C_{max} and R_s parameters for the batteries used when the onboard battery management software was started. The propulsion batteries were previously characterized by a slow discharge laboratory procedure, and then fitted to the equivalent circuit model using the Nelder-Mead method. More details are found in Bole et al., (2014).

4.1. Description of the Flight Experiment

A flight plan of timed airspeed segments at a fixed altitude (described in section 3.2) was also loaded into the onboard software. Only manual (stick-to-surface) pilot control commands were used to perform the test flights for this experiment. Aircraft propeller RPM, estimated battery SOC, and predictions of remaining flying time were displayed on a ground station display for the system operators in near real-time. The motor throttle was controlled by the pilot to attain each requested flight plan airspeed target. A second ground station operator called out the actual airspeed achieved and altitude as feedback to the pilot. The pilot adjusted the vehicle's airspeed to maintain the flight plan airspeed target values for the flight plan segment time duration as described in Section 3.2. These airspeed targets were all planned for constant altitude flight plan segments. An "Amber Warning" alarm was raised when the remaining flying time prediction came within two minutes of the 30% SOC landing limit threshold for the weakest battery. At the 2-minute "Amber Warning", the pilot was instructed to descend to landing approach pattern altitude and to be ready to begin the landing approach when the ground station displayed the "red alert". This indicated the lowest battery was at or below the 30% SOC limit threshold or that a low voltage (17.0V) safety limit threshold had been breached. The amber and red alerts are depicted in Fig. 8. Once the "red alert" threshold alarm was raised, an "End Research, Load Off" advisory status call was made to the pilot. The pilot then began the landing approach sequence and disarmed the parasitic load resistor bank. This precaution was necessary because the resistor bank generates sufficient heat to be a fire risk after several minutes without the cooling from the relative air movement of flight. Once landed, the motor was stopped and the vehicle was retrieved by ground personnel to prevent any additional battery consumption by ground taxiing. The battery data logging was continued for an additional twenty minutes after landing to document the recovery of the battery voltage that had been depressed due to the power demand to sustain flight. This battery voltage at near-equilibrium was used to compute an empirical approximation of the ending battery SOC based upon laboratory tests done at near-equilibrium (Bole et al., 2013). The data logging during the experimental flights was performed by the data system described in (Hogge et al., 2011).

4.2. Performance Requirements

The specification of performance requirements for verification of the remaining flying time predictions is described next. The predictive element tested is an alarm that warns system operators when the powertrain batteries are two minutes from reaching 30% SOC under normal operations.

Accuracy requirements for the two minute warning were specified as:

1. *The prognostic algorithm shall raise an alarm no later than two minutes before the lowest battery SOC estimate falls below 30% for at least 90% of verification trial runs.*
2. *The prognostic algorithm shall raise an alarm no earlier than three minutes before the lowest battery SOC estimate falls below 30% for at least 90% of verification trial runs.*
3. *There should be enough charge present in the batteries so as to complete at least 2 go-arounds in case of a missed landing.*

Here, the two minute alarm is biased to occur early rather than late since the landing becomes unsafe if not enough battery charge is present. The early alarm prediction bound limits the "opportunity cost" of unnecessarily denied flying time.

4. *Required confidence to specify when prognosis is sufficiently good* $-\beta > 50\%$

An additional requirement for the flying time prediction verification specifies maximum bounds on the ending SOC estimation error:

5. *The ending SOC estimation error as identified from the resting battery voltage must be less than 5% for at least 90% of verification trial runs.*

4.3. β Metric of Prediction Performance

Prognostic algorithms inherently contain uncertainties and often estimate the uncertainties in the predicted quantity. These estimates can be used to infer the variability (spread) in predictions. Figure 9 after Saxena et al. (2012) illustrates the β metric of the fraction of the probability mass falling between the two α bounds of acceptance. The higher the value of β, the higher the confidence that a prediction will remain within the two α bounds of acceptance. In Fig. 7 the

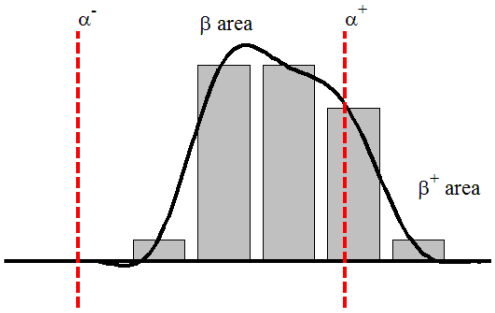

Figure 9. β Probability Density Function area within α acceptance limits.

portion enclosed between the α limits is the β percentage of the probability density function (PDF) contained between the limits. In this example β is 86%, or 86% of the PDF is within the α limits. The remaining portion outside the limits is referred to as β^+. A threshold criteria of 50% for the β metric for the prediction to be acceptable for decision making was proposed by Saxena, Roychoudhury, Celaya, Saha, Saha, and Goebel (2012). We use 50% for this test series.

Referring back to Fig. 7 the β values based upon histogram location before the parasitic load is engaged at time of 5 minutes are somewhat more than 50%. After the 5.0 minute time index, the histograms show that all the β density is contained within the α-bounds. The lower 50% bound on β works in conjunction with the α-bounds to specify performance constraints. As the α-bounds get narrower (i.e. less error tolerated) the probability density functions are required to contain the spread in order to satisfy the same β criterion. Figure 8 shows how the α error bounds narrow and the β histograms narrow as the 30% SOC threshold is approached. In the example shown here, the two-minute warning β histograms are all within the α bound limits implying a β of 100%. Referring back to Fig. 7 the prognostic horizon is somewhere before the beginning of the plot for the sample flight since even when the upper limit of the first few vertical bars is past the α^+ limit, the included portion is still greater than 50%. Figure 10 shows a cumulative plot of all the β values from 15 flight tests with the 50% pass/fail threshold dashed line. The flight that had a late prediction of the two-minute warning coincided with a β of less than 50%. In this run, the airspeed exceeded the target airspeed by as much as 17% due to the pilot's compensation for unsteady winds aloft and the desire to provide a larger margin above aircraft stall speed. The flight plan airspeed values were also not adjusted for this change in keeping with the experiment plan. An operator could want a β-derived status indicator that would indicate if the flying time predictions are reliable. However, since the β metric is calculated from the α bounds

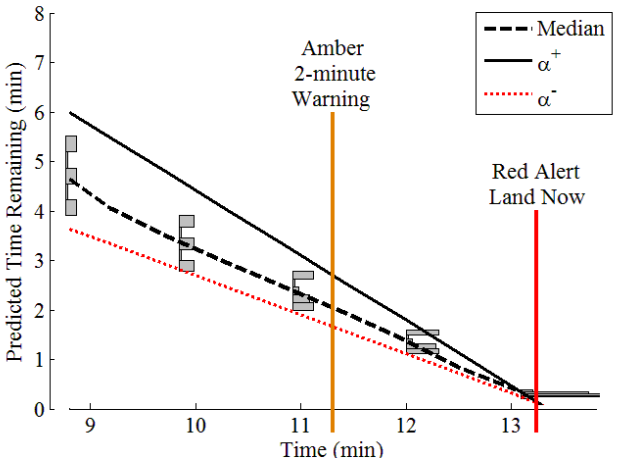

Figure 8. Advisory alarms with β PDF histograms of predictions

which is in turn based upon the ground truth time of the lowest battery crossing the 30% SOC threshold limit, and the ground truth SOC is calculated from a measurement taken 15 minutes after the landing, it is not available online and can only be computed offline well after the flight.

4.4. SOC Ground Truth

The definition of requirements 1, 2, and 4 stated previously in section 4.2 use the term "SOC estimate". The UKF state estimation algorithm described earlier, is relied upon to provide online *estimates* of battery SOC from measured battery current and voltages. A more direct measurement of battery SOC can be obtained after the experimental flight is complete by allowing the batteries to rest until the terminal voltage settles to a constant value. There is a known relationship between the equilibrium battery voltage and the SOC that can then be used to compute the ending SOC for all

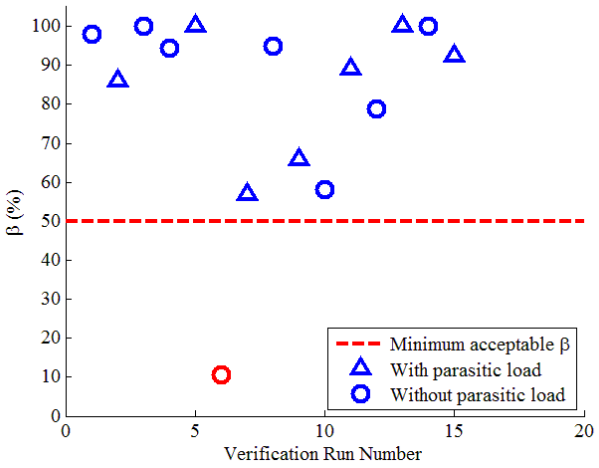

Figure 10. Passing β values for 15 flights

the powertrain batteries. The difference between the estimated battery SOC at the end of each flight and the measurement of SOC that is computed from the resting battery voltage is referred to here as the ending SOC estimation error. The allowed estimation error is specified in requirement five.

4.5. SOC Performance Results

Figure 11 shows box plots of the SOC estimation error measured over the 15 verification flights performed. Because each verification flight requires 4 powertrain batteries, 60 measurements of the SOC estimation error are produced. Eleven of these measurements fall outside of the 5% error tolerance allowed, thus only 82% of the trials pass. Requirement five that 90% of the trials stay within the 5% error benchmark was not satisfied. A goal of the flight test series was to use batteries with the same chemical formulation. However, there were not enough batteries with this formulation to support more than two flights a day. These batteries had identification numbers below 50. A few were of a different formulation with identification numbers 50 and above and were used for any third or fourth flights in a day. Change in the manufacturing batch leads to differences in chemical composition variability and manufacturing variability which is not completely modeled. Hence we observe some variation in the results discussed in this work. The batteries with the different formulation were characterized using the same method, and they seem to exhibit a similar range of variation as the majority batteries. This can be seen in the left half of Fig. 11. Since there are so few of them, the box plot quartiles collapse to the mean value for them.

Figure 12 shows that that the SOC of the lowest battery on the earliest flights were discharged well below the 30% target. The post flight SOC estimate approached the SOC 30% target as more flights were accomplished. This may be due to pilot acclimatization and a revised procedure introduced beginning verification flight number 4. The procedure change consisted of a preparatory descent to approach pattern altitude upon the two-minute warning to better position the airplane for landing before the 30% SOC "End Research, Load Off" call to land was given.

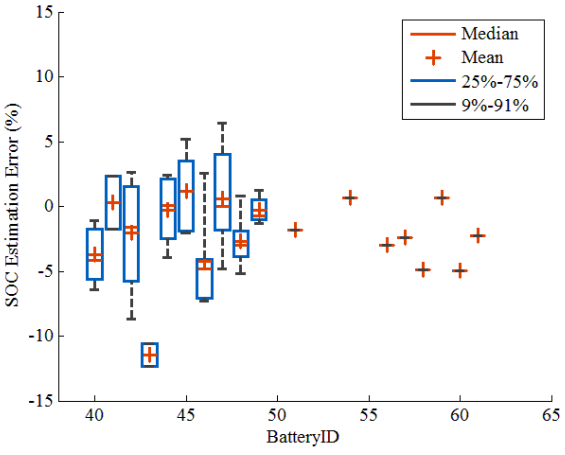

Figure 11. Box plots of the SOC estimation error measured over 15 verification flights that each use 4 batteries

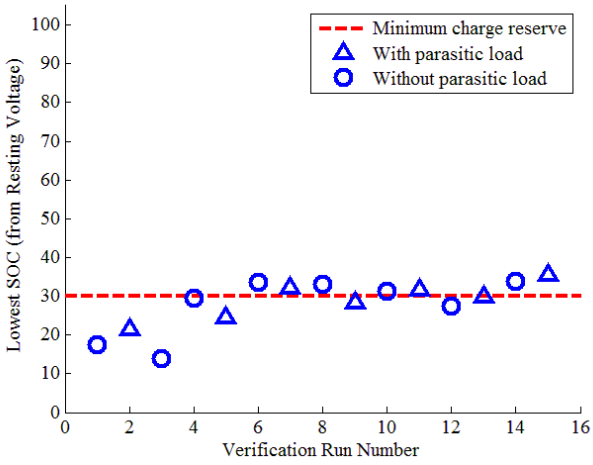

Figure 12.Lowest SOC from resting voltage recovery for 15 flights

4.6. Performance of Predicted Flying Time Warning

Figure 13 shows the difference between the time at which the two minutes remaining alarm was raised and the time at which the lowest battery SOC estimate crosses 30% for 15 verification flights, which includes flights that were performed with and without parasitic load injection. The vertical lines in the figure indicate the bounds on acceptable alarm accuracy. Looking at late prediction requirement 1, flight six's prediction of the two-minute warning was 0.2 min. late according to ground truth. One out of the 15 flights was predicted late or 93% not predicted late thus satisfying requirement one. Flight six also violated the $\beta > 50\%$ of requirement 4 and would not be considered reliable to inform decision making. One of the 15 flights was predicted more than three minutes early (flight 10). Since 93% were not predicted earlier than 3 minutes, requirement two was satisfied. Previous laboratory test chamber captive thrust tests discussed in Hogge et al., 2015, and Hogge, Bole, Vazquez, Kulkarni, Strom, Hill, Smalling and Quach, 2017 would cause the user to expect better performance. Some factors to consider between ground and flight testing are variation in the pilot's response to calm or windy environmental conditions. Pilot flying preference and "comfort level" varied more widely than was expected based upon experience with earlier parameter tuning flights with different pilots. Cool or warm days affect the battery initial temperature and parameters more than in the laboratory. Dry or humid days affect the air density "density altitude" and increase the

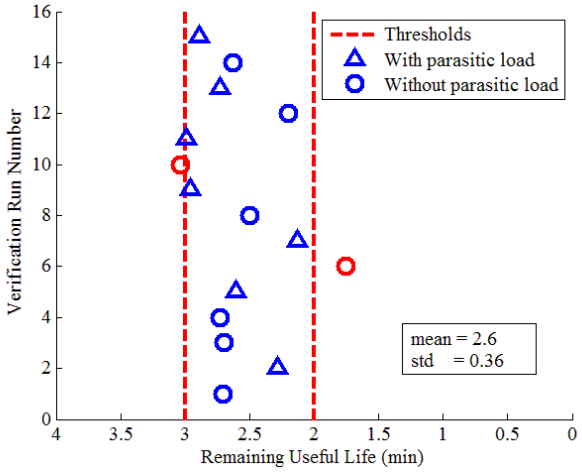

Figure 13. Two-minute alarms for 15 flights

energy demand necessary to maintain altitude. These sources of variation are not present in the laboratory tests.

Another question to be considered is how well do the repeated trials of the two-minute alarm indicate what we should expect for future flights? An Anderson-Darling test was run on the 15-flight data set of the two-minute warnings to test if the alarm times came from a Gaussian distribution. The test indicated that the alarm time predictions came from a normal distribution at the 5% significance level. Since the distribution is normal, a confidence interval test would be valid. The standard error of estimate of the two-minute alarm time given the sample mean is shown in Fig. 14. This figure repeats Fig. 13 except that the statistical measures are emphasized. The sample mean of the fifteen flights shows 2.6 minutes as the actual amber warning time as opposed to the specified range of 2 to 3 minutes for the 2-minute flying time remaining. The 95% confidence limits come from adding/subtracting two "standard error of estimate" values

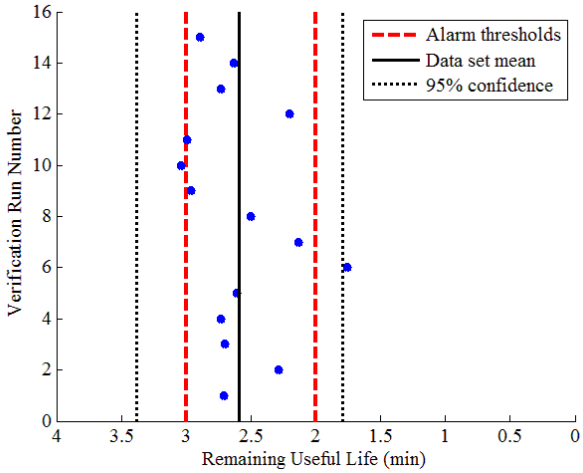

Figure 14. Two-minute alarms, 95% confidence limits

to/from the mean (Spiegel & Stephens, 1998). The numerical value for the standard error of estimate was 0.39 for this data set. The 95% confidence limits are biased to the early prediction side of the 2 to 3 minute alarm specification shown in the red dashed lines. This is to trade the opportunity cost of missed possible flying time against not having enough energy to repeat failed landing attempts. This trade-off was made empirically at the end of the series of flight tests since the initial tuning was based on captive-flight ground tests.

5. CONCLUSION

Flight tests to verify the performance of remaining flying time predictions for a small electric aircraft were described. Continued flight after aircraft battery packs have reached 30% SOC was defined as high risk operation for our experimental vehicle, and are to be avoided if possible. The flight tests did not pass the 5% ending SOC estimation error requirement but were not far from meeting that requirement (82% of 90%). The requirement that the two-minute warning alarm be satisfied 90% of the time was satisfied 93% of the time. Environmental and pilot variation are possible confounding factors and need to be better accounted for with an improved method. Repeatable testing such as that described in this paper is necessary to effectively debug, tune, and build trust in prognostic algorithms prior to deployment in mission critical applications.

ACKNOWLEDGEMENT

This work was funded by the NASA Shadow Mode Assessment using Realistic Technologies for the National Airspace System (SMART NAS) Program of the Aeronautics Research Mission Directorate (ARMD). Use of the Wireless Intelligent Sensing Electromagnetic Environmental Effects Research test chamber was appreciated. Allan White and Kenneth Eure are thanked for helpful suggestions and comments. Patrick Tae is thanked for his contribution to the testing of the parasitic load apparatus as part of his intern assignment. Samuel Bibelhauser is thanked for his contribution of a test chamber data logger used for ground tests as part of his intern assignment.

REFERENCES

Bole, B., Daigle, M., Gorospe, G.,. (2014). Online prediction of battery discharge and estimation of parasitic loads for an electric aircraft. *European Conference of the Prognostics and Health Management Society.*

Bole, B., Teubert, C., Quach, C., Hogge, E., Vazquez, S., Goebel, K., & Vachtsevanos, G. (2013). SIL/HIL replication of electric aircraft powertrain dynamics and inner-loop control for V&V of system health management routines. *Annual Conference of the Prognostics and Health Management Society.*

Ceraolo, M. (2000, November). New dynamical models of lead-acid batteries. *IEEE Transactions of Power Systems,* 15(4), 1184-1190.

Chen, M., & Rincon-Mora, G.A. (2006, June). Accurate electrical battery model capable of predicting runtime and I-V performance. *IEEE Transactions on Energy Conversion.* 21(2), 504-511.

Daigle, M., Saxena A. & Goebel, K. (2012). An efficient deterministic approach to model-based prediction uncertainty estimation. *Annual Conference of the Prognostics and Health Management Society, 2012.*

Ely, J., Koppen, S., Nguyen, T., Dudley, K., Szatkowski, G., Quach, C., Vazquez, S., Mielnik, J., Hogge, E., Hill, B. & Strom, T. (2011). *"Radiated Emissions From a Remote-Controlled Airplane - Measured in a Reverberation Chamber "*. NASA/TM-2011-217146.

Hogge, E., Bole, B., Vazquez, S., Celaya, J., Strom, T., Hill, B., Smalling, K. & Quach, C. (2015). Verification of a remaining flying time prediction system for small electric aircraft. *Annual Conference of the Prognostics and Health Management Society 2015.*

Hogge, E., Bole, B., Vazquez, S., Kulkarni, C., Strom, T., Hill, B., Smalling, K., & Quach, C. (2017). Verification of prognostic algorithms to predict remaining flying time for electric unmanned vehicles. to appear in *International Journal of Prognostics and Health Management, Vol. 8* doi: 2017

Hogge, E., Quach, C., Vazquez, S. & Hill, B. (2011). *"A Data System for a Rapid Evaluation Class of Subscale Aerial Vehicle"*. NASA/TM-2011-217145.

Julier, S. & Uhlmann, J. K. (1997). A new extension of the Kalman filter to nonlinear systems. In *Proceedings of the 11th international symposium on aerospace/defense sensing, simulation, and controls* (pp. 182-193)

Julier, S. & Uhlmann, J. (2004, March). Unscented filtering and nonlinear estimation. *Proceedings of the IEEE, 92(3), 401-422.*

Nelder, J. & Mead, R. (1965). A simplex method for function minimization. *Computer Journal* 1965; 7 (4), 308-313.

Quach, C., Bole, B., Hogge, E., Vazquez, S., Daigle, M., Celaya, J., Weber, A. & Goebel, K. (2013). Battery charge depletion prediction on an electric aircraft. *Annual Conference of the Prognostics and Health Management Society 2013.*

Saha, B., Koshimoto, E., Quach, C., Hogge, E., Strom, T., Hill, B., Vasquez, S. & Goebel, K. (2011). Battery health management system for electric UAV's. *IEEE Aerospace Conference.* Big Sky, MT.

Saha, B., Quach, C. & Goebel, K. (2012). Optimizing battery life for electric UAVs using a Bayesian framework. 2012 *IEEE Aerospace Conference.*

Saxena, A., Celaya, J., Saha, B., Saha, S. & Goebel, K. (2010). Metrics for offline evaluation of prognostic performance. *International Journal of Prognostics and Health Management, Vol. 1(1) 001, pp 13-15*, doi: 2010

Saxena, A., Roychoudhury, I., Celaya, J., Saha, B., Saha, S. & Goebel, K. (2012). Requirements flowdown for prognostics and health management. *Infotech@Aerospace Conference* (pp. 8-9). Garden Grove, CA: AIAA, Reston, VA.

Saxena, A., Roychoudhury, I., Lin, W. & Goebel, K. (2013). Towards requirements in systems engineering for aerospace IVHM design. *AIAA Conference, 2013.* AIAA, Reston, VA.

Spiegel, M. R. & Stephens, L. J., (1998). *Schaum's outline of theory and problems of statistics*. New York, NY: McGraw-Hill.

Zang, H., & Chow, M.-Y., (2010). Comprehensive dynamic battery modeling for PHEV applications. In IEEE power and energy society general meeting.

BIOGRAPHIES

Edward F. Hogge received a B.S. in Physics from the College of William and Mary in 1977. He has provided engineering services to the government and currently is employed by Northrop Grumman Technology Services. He has recently been supporting aviation safety research through the implementation of electronic systems for subscale remotely piloted aircraft and through commercial aircraft simulation. He is a member of the American Institute of Aeronautics and Astronautics.

Chetan S. Kulkarni received the B.E. (Bachelor of Engineering) degree in Electronics and Electrical Engineering from University of Pune, India in 2002 and the M.S. and Ph.D. degrees in Electrical Engineering from Vanderbilt University, Nashville, TN, in 2009 and 2013, respectively. He was a Senior Project Engineer with Honeywell Automation India Limited (HAIL) from 2003 till April 2006. From May 2006 to August 2007 he was a Research Fellow at the Indian Institute of Technology (IIT) Bombay with the Department of Electrical Engineering. From Aug 2007 to Dec 2012, he was a Graduate Research Assistant with the Institute for Software Integrated Systems and Department of Electrical Engineering and Computer Science, Vanderbilt University, Nashville, TN. Since Jan 2013 he has been a Staff Researcher with SGT Inc. at the Prognostics Center of Excellence, NASA Ames Research Center. His current research interests include physics-based modeling, model-based diagnosis and prognosis. Dr. Kulkarni is a member of the Prognostics and Health Management (PHM) Society, AIAA and the IEEE.

Sixto L. Vazquez Mr. Vazquez obtained MSEE from Old Dominion University in 1990 and BSEE from the University of Puerto Rico in 1983. He has developed real-time 3D graphical simulations to aid in the visualization and analysis of complex sensory data. He has developed techniques to interactively process, analyze, and integrate sensory data from multiple complex, state-of-the-art sensing technologies, i.e. FMCW Coherent Laser Radar range measuring system, Bragg grating Fiber Optic Strain Sensing system, etc., into simulation. In recent years, he has developed software for the Ardupilot and associated ground station.

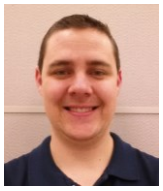

Kyle M. Smalling Kyle Smalling obtained his B.S. in Aerospace Engineering from Cal Poly Pomona in 2013. He is an avid remote control vehicle enthusiast both personally and professionally. His areas of research include Health Prognostics and developing Safety Critical hardware and software. He is employed by Northrop Grumman Technology Services.

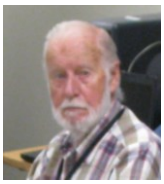

Thomas H. Strom was born in Aberdeen, WA, 1924. He graduated from Hoquiam High School in 1942, and attended Seattle University and the University of Washington 1953-1960. He served in the U.S. Navy during World War II as a Radar Technician. He was an employee of the Boeing Corp. Wind Tunnel, Seattle, WA 1947-1972. He was Senior Engineer with principal expertise in flutter and aeroelastic wind tunnel modeling. He was the founder and president of Dynamic Engineering, Inc., Newport News, VA, until 1987. He has served as a consultant to the Aeroelasticity Group of NASA Langley Research Center (LaRC) and continues to provide engineering and technical services to LaRC through Northrop Grumman Technology Services.

Cuong C. Quach received his M.S. from the School of Physics and Computer Sciences at Christopher Newport University in 1997. He is a staff researcher in the Safety Critical Avionics Systems Branch at NASA Langley Research Center. His research areas include development and testing of software for airframe diagnosis and strategic flight path conflict detection.